Electronic Supplementary Information (ESI)

High performance organic field-effect transistors based on single-crystal microribbons and microsheets of solution-processed dithieno[3,2-*b*:2',3'-*d*]thiophene derivatives

Yu Seok Yang,[a] Takuma Yasuda,*[a,b,c] Hayato Kakizoe,[a] Hiroyuki Mieno,[a] Hiori Kino,[d] Yoshitaka Tateyama,[c,d] and Chihaya Adachi*[a,b]

[a] Department of Applied Chemistry, Center for Organic Photonics and Electronics Research (OPERA), and [b] International Institute for Carbon Neutral Energy Research (WPI-I2CNER), Kyushu University, Japan

[c] PRESTO, Japan Science and Technology Agency (JST), Japan

[d] International Center for Materials Nanoarchitectonics, National Institute for Materials Science (NIMS), Japan

E-mail: yasuda@cstf.kyushu-u.ac.jp; adachi@cstf.kyushu-u.ac.jp

Table of Contents:

General. ^{1}H and ^{13}C NMR spectra were recorded on a Bruker Avance III 500 spectrometer. Chemical shifts of ^{1}H and ^{13}C NMR signals were quoted to tetramethylsilane (δ = 0.00) and $CDCl_3$ (δ = 77.0) as internal standards. Matrix-assisted laser desorption ionization time-of-flight (MALDI-TOF) mass spectra were collected on a Bruker Daltonics Autoflex III spectrometer using dithranol as the matrix. Elemental analyses were carried out with a Yanaco MT-5 CHN corder. UV/Vis absorption spectra were measured with a Shimadzu UV-2550 spectrometer. The HOMO energy levels were determined using a Riken-Keiki AC-3 ultraviolet photoelectron spectrometer. The LUMO energy levels were estimated by subtracting the optical energy gap (E_g) from the measured HOMO energy levels; the E_g values were determined from the onset position of the absorption spectra. The density-functional theory (DFT) calculations were performed on the Gaussian 03 program package, using the B3LYP functional with the 6-31G(d) basis set.[1] Thermogravimetric analysis (TGA) and differential scanning calorimetry (DSC) measurements were performed on a Shimadzu DTG-60AH at a scanning rate of 10 °C min^{-1} and a Netzsch DSC204 Phoenix calorimeter at a scanning rate of 5 °C min^{-1}, respectively, under N_2 atmosphere. AFM was performed using a JEOL JSPM-5400 scanning probe microscope with tapping-mode in air. X-ray crystallographic analyses were made on a Rigaku VariMax with a Saturn 724+ system with graphite monochromated Mo*K*α radiation. The structures were solved by direct methods (SIR2008)[2] and refined by full-matrix least-square techniques based on F^2 (SHELXL-97).[3]

OFET Device Fabrication and Measurements. **DTT-8** and **DTT-12** were incorporated into OFETs with a bottom-gate and top-contact geometry. Single-crystal microribbons or microsheets of **DTT-8** and **DTT-12** were grown by drop-casting method. For all of the OFET devices, heavily doped *n*-type Si wafers with a thermally grown 300-nm-thick SiO_2 layer were used as substrates. The SiO_2/Si substrates were pretreated with a piranha solution at 90 °C for 0.5 h, and then copiously cleaned by sonication in deionized water, acetone, and isopropanol in that order. Next, an approximately 30-nm-thick poly(methylmethacrylate) (PMMA) thin layer was dip-coated onto the SiO_2/Si substrates as an additional dielectric to reduce charge trapping by the silanol groups on SiO_2 in the final devices. Single crystals were

fabricated by drop-casting from a 0.4–1.0 mg/mL solution of **DTT-8** or **DTT-12** in 1,2-dichlorobenzene (DCB) onto the PMMA-coated SiO_2/Si substrates, where the PMMA can also help to make the drop-casting solution spread well on the substrate and facilitate molecular self-organization during the fabrication process, providing superior quality crystals. The drop-cast solutions were then dried for 12 h in a dry nitrogen-filled glove box at room temperature. The devices were completed by evaporating gold (thickness = 50 nm) through a shadow mask to define the source and drain electrodes with a channel length of 20–100 μm on top of each single-crystal microribbon or microsheet. The output and transfer characteristics of the OFETs were measured using an Agilent B1500A semiconductor parameter analyzer under ambient conditions at room temperature. Field-effect mobilities (μ) of the OFETs were calculated in the saturation regime using the following equation: $I_D = (W/2L)\mu C_i(V_G-V_{th})^2$, where I_D is the source–drain current, W and L are channel width and length, respectively, C_i is the capacitance per unit area of the gate dielectric (10.9 nF/cm^2), V_G is the gate voltage, and V_{th} is the threshold voltage.

Band Structure Calculations. We have used the DFT with PBE functional implemented in the QMAS code. The experimental values are used for the unit cell (for **DTT-8**: *Cmc*2_1, a = 70.25 Å, b = 7.333 Å, c = 5.822 Å; for **DTT-12**: *Cmc*2_1, a = 88.90 Å, b = 7.391 Å, c = 5.846 Å) and the atomic coordinates. They were not optimized because van der Waals interaction is expected to be main cohesive source among the alkyl chains, whereas the terminating H atoms are relaxed. The wavefunction optimizations were carried out with 4×4×8 k points and 40 Ry of the cutoff energy in the PAW formalism. With the optimized charge density, we have carried out the band structure calculations along the representative directions.

Materials and Syntheses. Commercially available reagents and solvents were used without further purification unless otherwise noted. All of the reactions were performed under a nitrogen atmosphere in dry solvents using standard Schlenk techniques. The synthetic routes for **DTT-8** and **DTT-12** are outlined in Scheme S1. 2-(4-Octylphenyl)-4,4,5,5-tetramethyl-[1,3,2]dioxaborolane (**2a**) and 2-(4-dodecyl-phenyl)-4,4,5,5-tetramethyl-[1,3,2]dioxaborolane (**2b**) were prepared according to the

literature procedure,[4] and were obtained as colorless oils in 92% and 65% yields, respectively. Dithieno[3,2-*b*:2',3'-*d*]thiophene (**3**) was purchased from Aldrich. The final products were fully characterized by ^{1}H and $^{13}C\{^{1}H\}$ NMR spectroscopy, MALDI-TOF mass spectrometry, and elemental analysis, as described below.

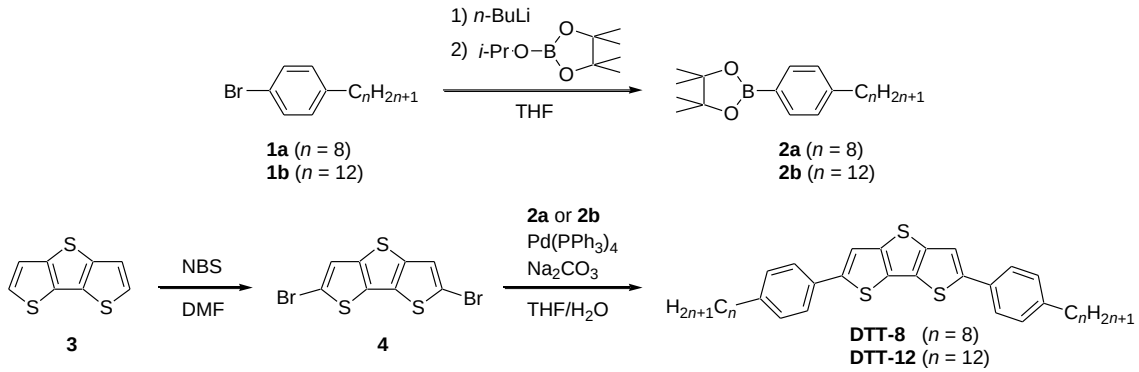

Scheme S1. Synthesis of **DTT-8** and **DTT-12**.

Synthesis of 2,6-dibromo-dithieno[3,2-*b*:2',3'-*d*]thiophene (4). To a stirred solution of **3** (2.47 g, 12.5 mmol) in dry DMF (50 mL) was added slowly *N*-bromosuccinimide (NBS, 4.57 g, 25.7 mmol) at 0 °C. The mixture was allowed to warm up to room temperature and stirred overnight. The reaction mixture was poured into water to form a precipitate. The precipitate was collected by filtration and washed with methanol. The product was recrystallized from $CHCl_3$/methanol and dried under vacuum to give **4** as an off-white solid (yield = 4.20 g, 95%). M.p. 171 °C. ^{1}H NMR (500 MHz, $CDCl_3$): δ 7.28 (s, 2H). $^{13}C\{^{1}H\}$ NMR (125 MHz, $CDCl_3$): δ 139.11, 130.88, 123.23, 112.38. MS (MALDI-TOF): *m*/*z* 353.64 $[M]^{+\cdot}$. Anal. calcd (%) for $C_8H_2Br_2S_3$: C 27.13, H 0.57; found: C 27.38, H 0.61.

Synthesis of 2,6-bis(4-octylphenyl)-dithieno[3,2-*b*:2',3'-*d*]thiophene (DTT-8). To a mixture of **2a** (5.57 g, 17.6 mmol) and **4** (2.83 g, 8.0 mmol) in dry THF (60 mL) were added $Pd(PPh_3)_4$ (0.92 g, 0.8 mmol) and aqueous Na_2CO_3 (2.0 M, 30 mL; Ar bubbled before use). The mixture was vigorously stirred for 24 h at 60 °C. After cooling to room temperature, the reaction mixture was poured into water, and then extracted with $CHCl_3$. The combined organic layers were washed with water, and dried over anhydrous Na_2SO_4. After filtration and evaporation, the product was purified by silica gel column chromatography (eluent: $CHCl_3$), recrystallized from $CHCl_3$/methanol, and

dried under vacuum to afford **DTT-8** as a yellow solid (yield = 4.08 g, 89%). This compound was further purified by repetitive temperature-gradient sublimation before use. Phase transition behavior: Cr 57 °C SmX 190 °C SmC 211 °C N 219 °C Iso (Abbreviations: Cr, crystalline; SmX, unidentified ordered smectic; SmC, smectic C; N, nematic; Iso, isotropic phase). ^{1}H NMR (500 MHz, $CDCl_3$): δ 7.55 (d, J = 7.8 Hz, 4H), 7.47 (s, 2H), 7.22 (d, J = 7.8 Hz, 4H), 2.63 (t, J = 7.7 Hz, 4H), 1.67-1.60 (m, 4H), 1.35-1.25 (m, 20H), 0.88 (t, J = 6.6 Hz, 6H). ^{13}C{^{1}H} NMR (125 MHz, $CDCl_3$): δ 145.23, 142.99, 141.50, 132.01, 130.00, 129.11, 125.63, 116.02, 35.71, 31.90, 31.40, 29.49, 29.33, 29.27, 22.68, 14.10. MS (MALDI-TOF): m/z 572.15 $[M]^{+\cdot}$. Anal. calcd (%) for $C_{36}H_{44}S_3$: C 75.47, H 7.74; found: C 75.42, H 7.69.

Synthesis of 2,6-bis(4-dodecylphenyl)-dithieno[3,2-*b*:2',3'-*d*]thiophene (DTT-12). This compound was prepared in a fashion similar to **DTT-8**, using **2b** (1.82 g, 4.9 mmol), **3** (0.78 g, 2.2 mmol), and $Pd(PPh_3)_4$ (0.17 g, 0.15 mmol). The product was obtained as a yellow solid (yield = 1.30 g, 86%). This compound was further purified by repetitive temperature-gradient sublimation before use. Phase transition behavior: Cr 83 °C SmX_1 119 °C SmX_2 167 °C N 194 °C Iso. ^{1}H NMR (500 MHz, $CDCl_3$): δ 7.55 (d, J = 8.2, 4H), 7.46 (s, 2H), 7.22 (d, J = 8.2 Hz, 4H), 2.63 (t, J = 7.8 Hz, 4H), 1.67-1.60 (m, 4H), 1.35-1.25 (m, 36H), 0.88 (t, J = 6.8 Hz, 6H). ^{13}C{^{1}H} NMR (125 MHz, $CDCl_3$): δ 145.25, 143.00, 141.53, 132.03, 130.03, 129.11, 125.63, 116.02, 35.71, 31.94, 31.40, 29.68, 29.66, 29.61, 29.53, 29.37, 29.32, 22.70, 14.12. MS (MALDI-TOF): m/z 684.34 $[M]^{+\cdot}$. Anal. calcd (%) for $C_{44}H_{60}S_3$: C 77.13, H 8.83; found: C 77.06, H 8.79.

References

1 (*a*) C. Lee, W. Yang, and R. G. Parr, *Phys. Rev. B*, 1988, **37**, 785; (*b*) P. C. Hariharan and J. A. Pople, *Chem. Phys. Lett.*, 1972, **16**, 217; (*c*) P. C. Hariharan and J. A. Pople, *Theor. Chim. Acta*, 1973, **28**, 213.

2 M. C. Burla, R. Caliandro, M. Camalli, B. Carrozzini, G. L. Cascarano, L. De Caro, C. Giacovazzo, G. Polidori, D. Siliqi, and R. Spagna, *J. Appl. Cryst.*, 2007, **40**, 609.

3 G. M. Sheldrick, *Programs for Crystal Structure Analyses (Release 97-2)*, University of Göttingen, Germany, 1997.

4 M. Sonntag and P. Strohriegl, *Tetrahedron Lett.*, 2006, **47**, 8313.

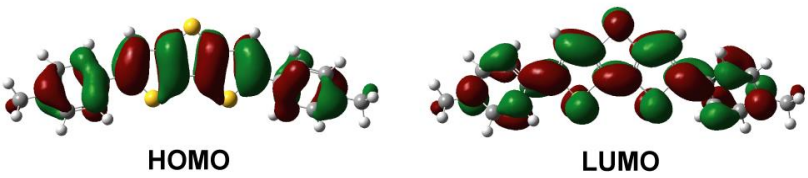

Fig. S1. Frontier orbital distributions for the π-conjugated core of the molecules calculated at the B3LYP/6-31G(d) level. The calculated HOMO/LUMO energies are −5.30/−1.73 eV, respectively.

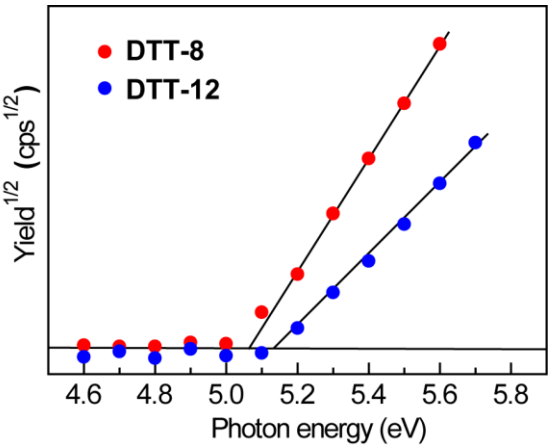

Fig. S2. Photoelectron yield spectra of thin films of **DTT-8** and **DTT-12**.

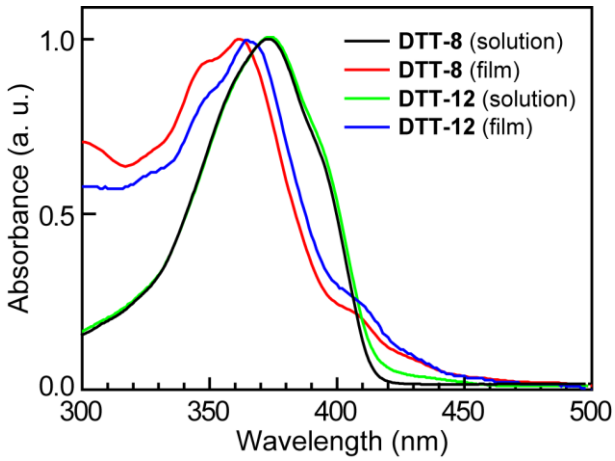

Fig. S3. UV/vis spectra of **DTT-8** and **DTT-12** in CH_2Cl_2 solution and thin films.

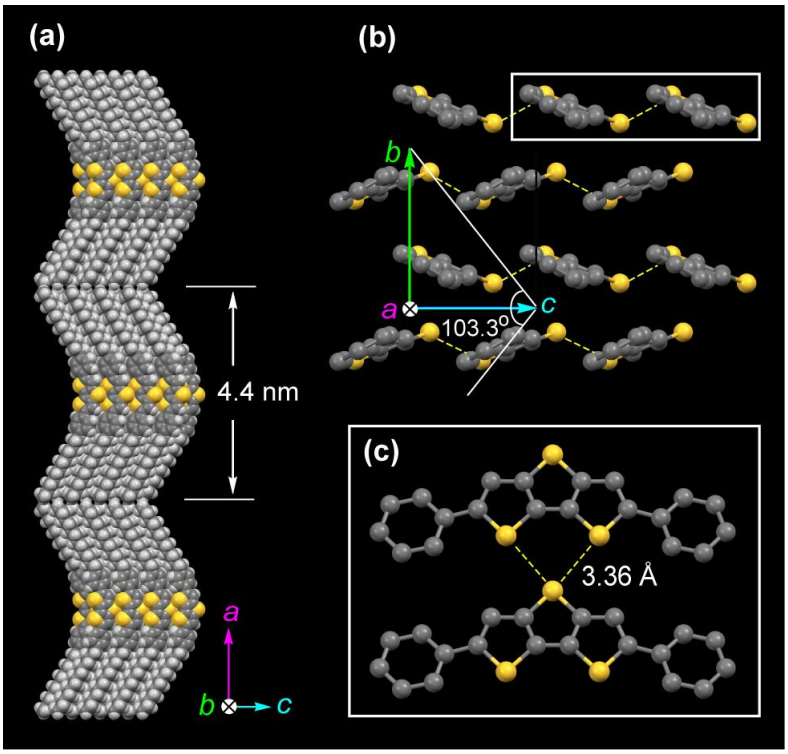

Fig. S4. (a) Space-filling representation of the crystal structure of **DTT-12**, showing layer-by-layer molecular association along the *a*-axis, which is normal to the substrate. (b) Herringbone molecular arrangement in the *b*–*c* plane. The dashed lines denote the close intermolecular S···S contacts. Note that the angle between the (011) and (−101) planes (θ = 103.3°) coincides with the angle of the facets at the crystal edge in the microscope image (Fig. 1b), indicating that the fastest crystal-growth direction is along the *c*-axis. (c) Magnified view for two neighboring molecules linked through double S···S contacts, projected along the *b*-axis. Dodecyl groups and hydrogen atoms are omitted for clarity.

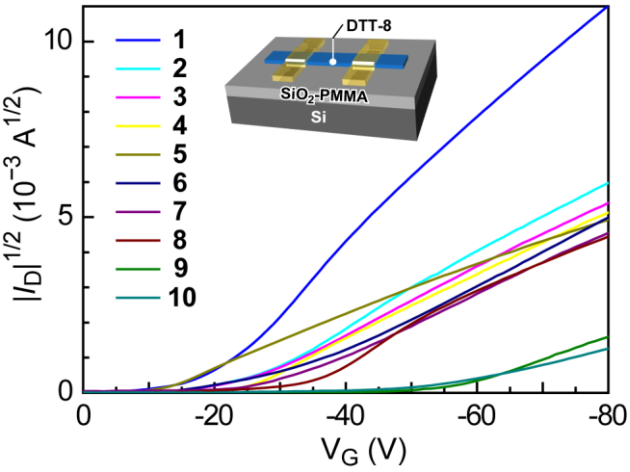

Fig. S5. Transfer characteristics of OFETs based on **DTT-8** microribbons. The data for 10 individual devices are presented (see also Table S1 for details).

Table S1. Summary of OFET properties of **DTT-8** microribbons[a]

Device	W (μm)	L (μm)	μ_{FET} (cm^2/Vs)	V_{th} (V)	I_{on}/I_{off}
1	17.7	38.6	10.2	−22	10^7
2	19.7	43.0	3.8	−25	10^7
3	9.4	42.3	7.0	−25	10^7
4	21.2	51.3	3.5	−24	10^7
5	11.5	59.5	4.3	−12	10^7
6	21.1	50.2	4.0	−29	10^6
7	16.2	39.5	3.4	−29	10^5
8	19.8	42.1	3.9	−34	10^6
9	9.6	67.0	5.5	−55	10^6
10	3.8	68.1	6.5	−48	10^7

[a]Abbreviations: W = channel width; L = channel length; μ_{FET} = hole mobility; V_{th} = threshold voltage determined by extrapolating the $|I_D|^{1/2}$ vs. V_G plot to I_D = 0; I_{on}/I_{off} = on/off ratio determined from the I_D at V_G = 0 V (I_{off}) and V_G = −80 V (I_{on}).

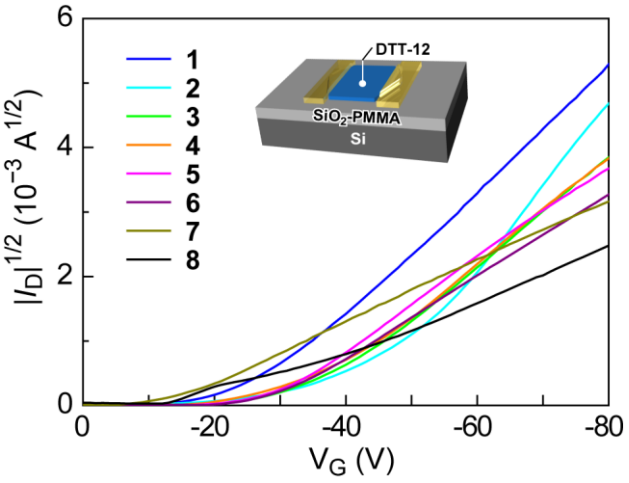

Figure S6. Transfer characteristics of OFETs based on **DTT-12** microsheets. The data for 8 individual devices are presented (see also Table S2 for details).

Table S2. Summary of OFET properties of **DTT-12** microsheets[a]

Device	W (μm)	L (μm)	μ_{FET} (cm^2/Vs)	V_{th} (V)	I_{on}/I_{off}
1	54.3	54.7	1.81	−26	10^5
2	69.2	21.6	1.01	−43	10^5
3	118.0	49.9	0.57	−35	10^6
4	104.6	53.4	0.65	−36	10^6
5	60.1	41.2	0.60	−31	10^6
6	65.0	90.7	1.00	−30	10^5
7	41.1	72.0	0.75	−16	10^5
8	52.2	42.1	0.65	−25	10^4

[a]Abbreviations: W = channel width; L = channel length; μ_{FET} = hole mobility; V_{th} = threshold voltage determined by extrapolating the $|I_D|^{1/2}$ vs. V_G plot to I_D = 0; I_{on}/I_{off} = on/off ratio determined from the I_D at V_G = 0 V (I_{off}) and V_G = −80 V (I_{on}).

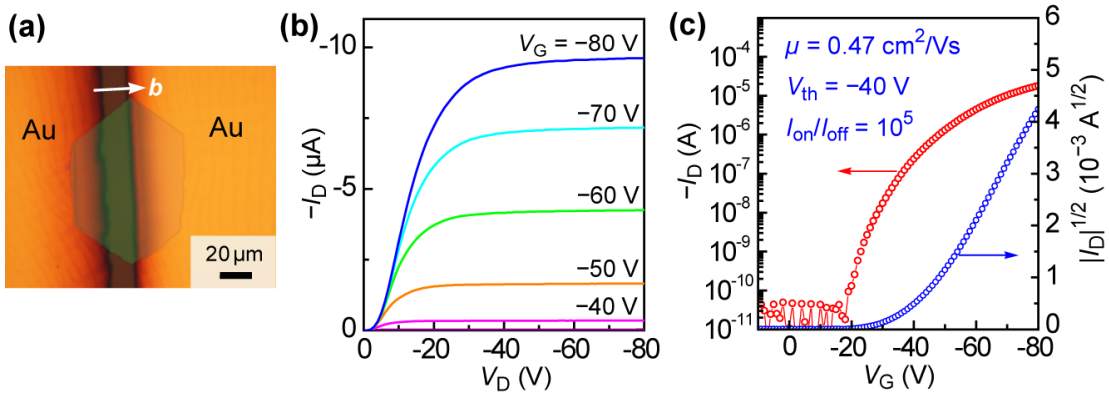

Figure S7. Single-crystal OFET properties of **DTT-12** microsheet along the *b*-axis: (a) optical micrograph, (b) output, and (c) transfer characteristics of the device.

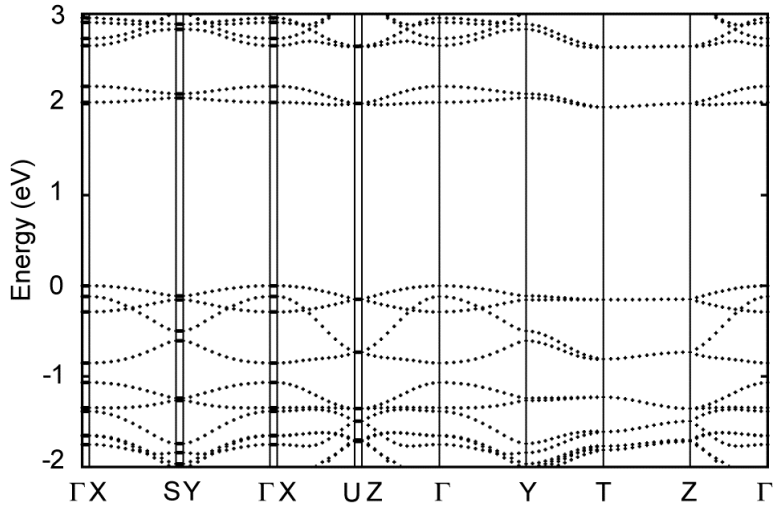

Figure S8. Electronic band structure of the **DTT-12** single crystal. The points of high symmetry in the first Brillouin zone are labelled as Γ = (0, 0, 0), X = (0.5, 0, 0), Y = (0, 0.5, 0), Z = (0, 0, 0.5), S = (0.5, 0.5, 0), T = (0, 0.5, 0.5), U = (0.5, 0, 0.5) in crystallographic coordinates. The dispersion characteristics and bandwidth in the uppermost valence band of **DTT-12** are similar to those of **DTT-8**; however, the degeneracy in the HOMOs is lost for the **DTT-12** crystal.